Chapter 5

EFFECT OF CORNER MODIFICATIONS ON ALONG AND ACROSS WIND LOAD OF A SQUARE BUILDING USING CFD ANALYSIS

5.1 Introduction

Tall buildings face a significant challenge when it comes to wind loads. Therefore, it is crucial to accurately assess wind loads in the design of these structures. One effective strategy for tackling this issue is through aerodynamic modifications. This research aims to investigate how well aerodynamic adjustments like corner modifications work on a square-shaped model using computational fluid dynamics (CFD) simulations conducted with the ANSYS Fluent software. The modifications made to the corners include chamfering, rounding, recessing, and double recessing. In each of these corner modification techniques, an additional four models are created. In these models, the length of each side of the square is reduced by 5%, 10%, 15%, and 20%. This results in a total of sixteen different models with corner modifications. The research begins with validating the square model, ensuring its accuracy, and after that, simulations are conducted for all sixteen models. To assess the effectiveness of the modifications, force and pressure coefficients are employed as indicators of along wind load and lift coefficient is an indicator of across wind load. The outcomes of these simulations are presented and discussed in the results and discussion section.

5.2 Modelling

The assessment carried out in this research relies on the outcomes of Computational Fluid Dynamics (CFD) simulations. To construct three-dimensional computational domain of the building, Space Claim software was employed. ANSYS design modeler facilitated

the creation of models for the wind tunnels that were integral to this study. The simulation of wind tunnel experiments was executed using ANSYS Fluent. The resultant simulated wind forces were subsequently harnessed to measure the pressure on the buildings model.

5.3 Description of models

The study encompasses a total of seventeen building models. Among these, the base model takes a square shape in its plan and possesses dimensions with a ratio of 1:1:2, as depicted in Figure 5.1. The research explores four distinct corner modification approaches: chamfered, rounded, recessed, double-recessed. These strategies are visually represented in the plan view shown in Figure 5.2. Each of these corner modifications entails an additional set of four models, wherein every side of the square experiences reductions of 5%, 10%, 15%, and 20% in its length at the corners as shown in Table 5.1. This results in a total sixteen corner-modified models.

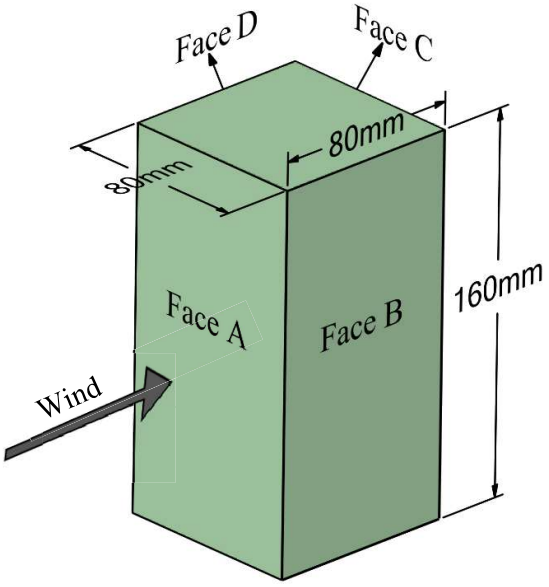

Figure 5.1 Details of Base Model/Square model

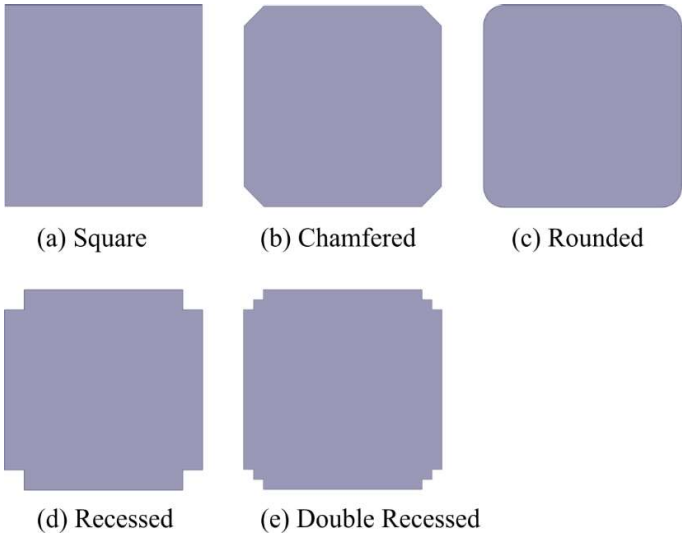

Figure 5.2 Plan view of base and corner modification models. **a.** Square **b.** Chamfered **c.** Rounded **d.** Recessed **e.** Double Recessed

Table 5.1 Corner modification models opted for the study

Reduction (%)	Chamfered	Rounded	Recessed	Double Recessed
5%				
10%				
15%				
20%				

In this study, the focus is on simulating the airflow around an isolated high-rise building. To validate the accuracy of our simulations, we draw upon the meticulous flow field measurements conducted by Meng and Hibi (1998) within a wind tunnel. These measurements were conducted under the influence of an urban atmospheric boundary layer. Importantly, the findings of Meng and Hibi (1998) have been endorsed as a benchmark for validation in the guidelines established by the Architectural Institute of Japan and widely used in the field of computational wind engineering.

5.4 Computational domain and boundary conditions

The wind tunnel is structured as a rectangular enclosure with dimensions of 21*b* x 13.75*b* x 11.25*b*, *b* is the side dimension of the building model, *b*=80 *mm* and *h*=2*b* ,*i.e.,* (Figure 5.1) resembling the experimental setup of Meng and Hibi (1998),. Boundary conditions encompass a velocity inlet at the domain's entrance, a pressure outlet with zero static pressure at the exit, a no shear wall for the ground, and free slip walls for three sides; building walls adhere to a no-slip condition (Liu and Niu 2016) as shown in Figure 5.3. The evaluated Reynolds number is 2.4 x 10^4 determined by building height (h) and inflow velocity (u_h) at $z = h$, with vertical profiles of mean velocity (u) and turbulent kinetic energy (k) adopted as per AIJ recommendations. The resulting blockage ratio, 1.3%, is well below the 3% limit suggested by Franke *et al*. (2007), indicating nominal obstruction from the building within this computational wind tunnel setup.

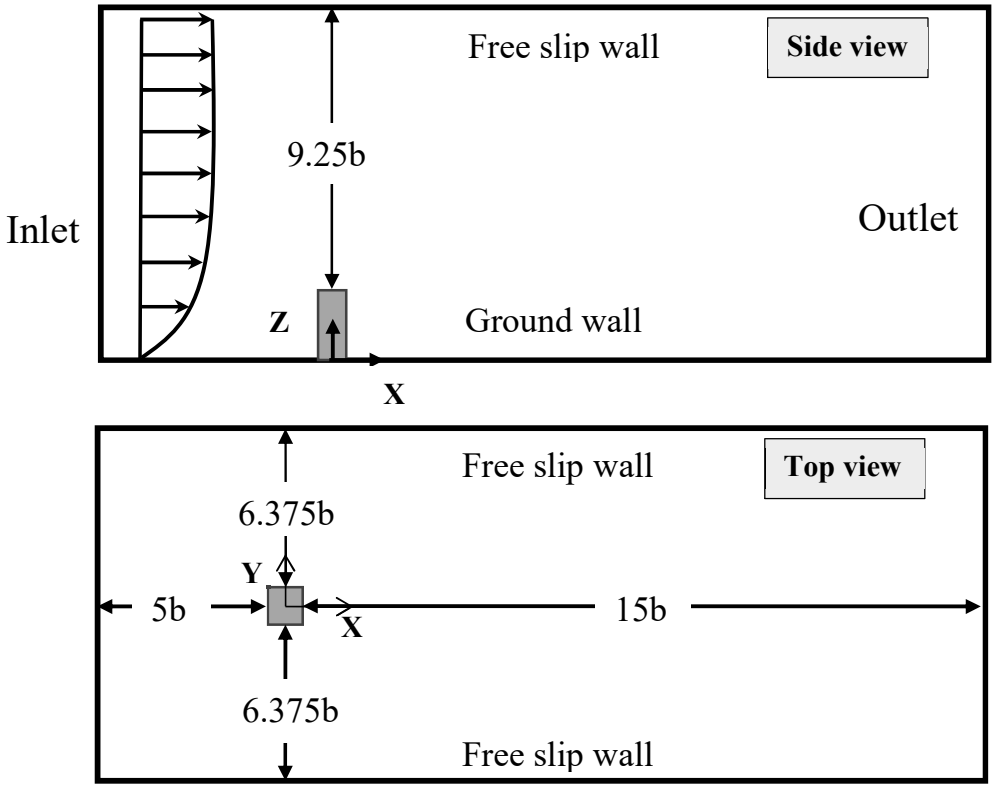

Figure 5.3 Side view and Top view of computational domain

The variable "*k*" represents turbulence kinetic energy, defined as the variance of velocity fluctuations, and it carries dimensions of (L^2T^{-2}), for instance, m^2/s^2. Whereas, "ε" signifies turbulent eddy dissipation, measured in dimensions of per unit time (L^2T^{-3}), such as m^2/s^3. Notably, the *k*-ε model introduces two fresh variables into the system of equations, expanding the scope of analysis and enhancing the precision of CFD simulations. Equation (5.1) depicts the continuity equation and Equation (5.2) shows the momentum equation (Jones and Launder (1972), Rodi(1980), Haggkvist *et al.* (1989)).

$$\frac{\partial \rho}{\partial t} + \frac{\partial}{\partial x_j}\left(\rho U_j\right) = 0 \tag{5.1}$$

$$\frac{\partial \rho U_i}{\partial t} + \frac{\partial}{\partial x_j}\left(\rho U_i U_j\right) = -\frac{\partial p'}{\partial x_j} + \frac{\partial}{\partial x_j}\left[\mu_{eff}\left(\frac{\partial U_i}{\partial x_j} + \frac{\partial U_j}{\partial x_i}\right)\right] + S_M \tag{5.2}$$

Where, S_M = Sum of body forces; μ_{eff} = effective viscosity accounting for turbulence; p' = modified pressure, defined in Equation (5.3)

$$p' = p + \frac{2}{3}\rho k + \frac{2}{3}\mu_{eff}\frac{\partial \rho U_k}{\partial k} \tag{5.3}$$

The last term in Equation (5.3) involves the divergence of velocity. It is neglected in fluent solver. Therefore, this assumption is strictly correct only for incompressible fluids. The k-ε model is based on the eddy viscosity concept as shown in Equation (5.4)

$$\mu_{eff} = \mu + \mu_t \tag{5.4}$$

Where, μ is molecular viscosity and, μ_t is the turbulent viscosity. The $k-\varepsilon$ model assumes that the turbulence viscosity is linked to the turbulence kinetic energy and dissipation through the relation:

$$\mu_t = C_\mu \rho \frac{k^2}{\varepsilon} \tag{5.5}$$

The values of k and ε come directly from the differential transport equations for the turbulence kinetic energy and turbulence dissipation rate as shown in Equation (5.6) and Equation (5.7).

$$\frac{\partial(\rho k)}{\partial t} + \frac{\partial}{\partial x_j}(\rho k U_j) = \frac{\partial}{\partial x_j}\left[\left(\mu + \frac{\mu_t}{\sigma_k}\right)\frac{\partial k}{\partial x_j}\right] + P_k + P_b - \rho\varepsilon - Y_M + S_k \tag{5.6}$$

$$\frac{\partial(\rho \varepsilon)}{\partial t} + \frac{\partial}{\partial x_j}(\rho \varepsilon U_j) = \frac{\partial}{\partial x_j}\left[\left(\mu + \frac{\mu_t}{\sigma_\varepsilon}\right)\frac{\partial \varepsilon}{\partial x_j}\right] + \rho C_1 S_\varepsilon - \rho C_2 \frac{\varepsilon^2}{k + \sqrt{\nu\varepsilon}} - C_{1\varepsilon}\frac{\varepsilon}{k}C_{3\varepsilon}P_b + S_\varepsilon \tag{5.7}$$

Where, C_1=max $[0.43, \frac{\eta}{\eta+5}]$, $\eta = S\frac{k}{\varepsilon}$, $S = \sqrt{2S_{ij}S_{ij}}$

Here, we have distinct elements to consider: P_k represents the generation of turbulence kinetic energy resultant from mean velocity gradients; P_b stands for the generation of

turbulence kinetic energy caused by buoyancy effects; and Y_M denotes the contribution of fluctuating dilatation in compressible turbulence to the overall dissipation rate. These components collectively shape the characteristics of wind flow dynamics. In the context of the *k-ε* turbulence model, specific constants hold significance: $C_{1\varepsilon}$, set at 1.44, signifies a model constant; similarly, C_2, at 1.92 (Rodi 1980), is another pivotal constant. Furthermore, the turbulence model constants for the *k* equation are denoted by σ_k (set at 1.0) and for the *ε* equation by σ_ε (set at 1.2). This comprehensive arrangement contributes to the workings of the *k-ε* turbulence model, shaping its behaviour within CFD analysis.

The velocity profile of the atmospheric boundary layer in the CFD is calculated by the power law as shown in Equation (5.8).

$$U(z) = U_H \times \left(\frac{z}{z_H}\right)^{\alpha} \tag{5.8}$$

Where U(z) is the velocity at height 'z' above ground, U_H is the speed at the reference elevation z_H which is 4.491 *m/s* in this study α is the power law coefficient, which is taken as 0.27 (for urban area). The kinetic energy (*k*) of the turbulence and its dissipation rate (*ε*) at the inlet section is calculated according to Equation (5.9) and Equation (5.10).

$$k = A_1\left(\frac{z}{b}\right)^3 + A_2\left(\frac{z}{b}\right)^2 + A_3\left(\frac{z}{b}\right) + A_4 \tag{5.9}$$

$$\varepsilon = C_\mu^{0.75}\left(\frac{k^{1.5}}{l}\right) \tag{5.10}$$

Where A_1=0.0042, A_2= -0.0719, A_3= 0.2693 and A_4 =0.3671, *b* is side dimension of model (80 *mm*), *l* is the characteristics length, C_μ is constant having value 0.09 (Richards and Hoxey (1993)).

5.5 Validation of profile

The validation process involves confirming the accuracy of the generated velocity profile to ensure the credibility of the undertaken work. To achieve this, the simulated velocity profile is cross-referenced with the one produced through the utilization of the power law equation, as outlined by Liu and Niu (2016). By referring to Figure 5.4, it becomes evident that the simulated profile aligns remarkably well with the profile generated using the power law equation, demonstrating a level of accuracy that is considered satisfactory. This, in turn, enables us to assert that the flow characteristics employed as part of this study hold a valid and acceptable status.

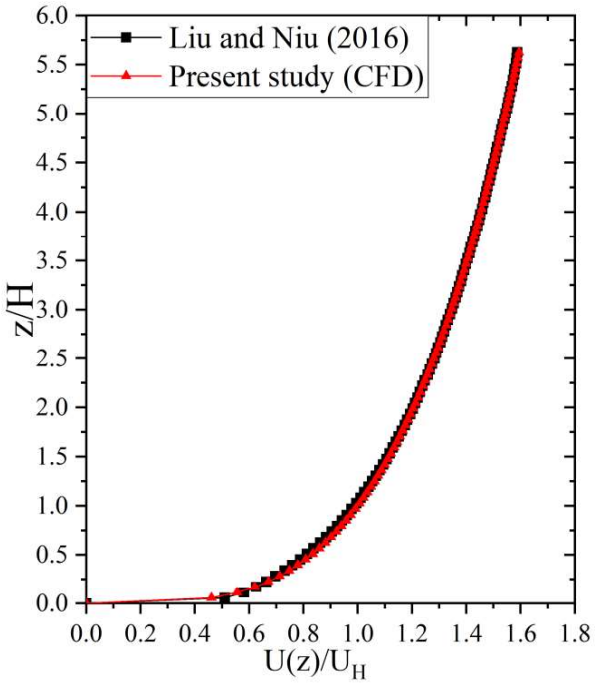

Figure 5.4 Velocity profile diagram

5.6 Methodology

This section outlines the methodology employed for the comprehensive investigation of building models through the utilization of ANSYS Fluent software. The research involves the application of four primary corner modification techniques: chamfered, recessed,

double-recessed, and rounded corners. The research methodology follows a systematic process as visualized in Figure 5.5. This flow diagram succinctly captures the sequential steps undertaken during the analysis in ANSYS Fluent. SIMPLEC algorithm is utilized. Discretization scheme used for the convection and diffusion terms was the second order upwind scheme. Residuals are kept less than 10^{-5}.

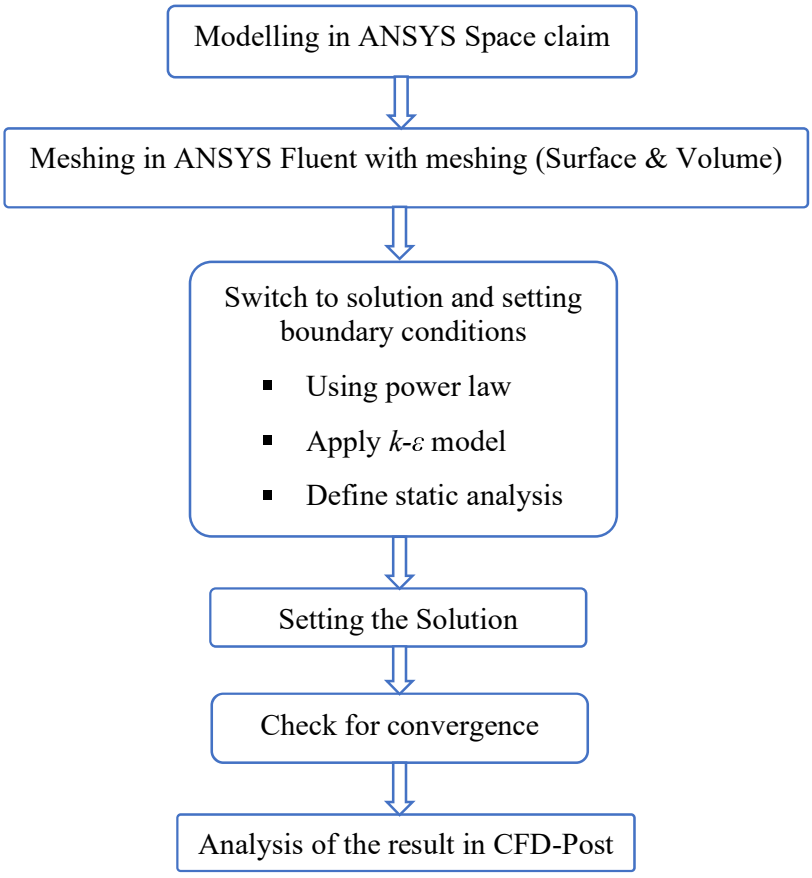

Figure 5.5 Flow chart of ANSYS Fluent to solve the analytical model

5.7 Details of meshing

The quality of the mesh is a critical factor in determining the accuracy of simulation outcomes, although achieving it is a complex task. Over the past twenty years, diverse types of meshes have emerged, among which structured (hexahedral) and unstructured (tetrahedrons and prisms) meshes have gained prominence in computational fluid

dynamics (CFD) simulations. These mesh varieties play a pivotal role in ensuring reliable and precise simulation results. In this study, poly-hexacore meshing is used with cell growth rate 1.08. The non-dimensional wall distance y^+ of the first near wall grids was kept less than 5. The meshing of the base model is shown in Figure 5.6.

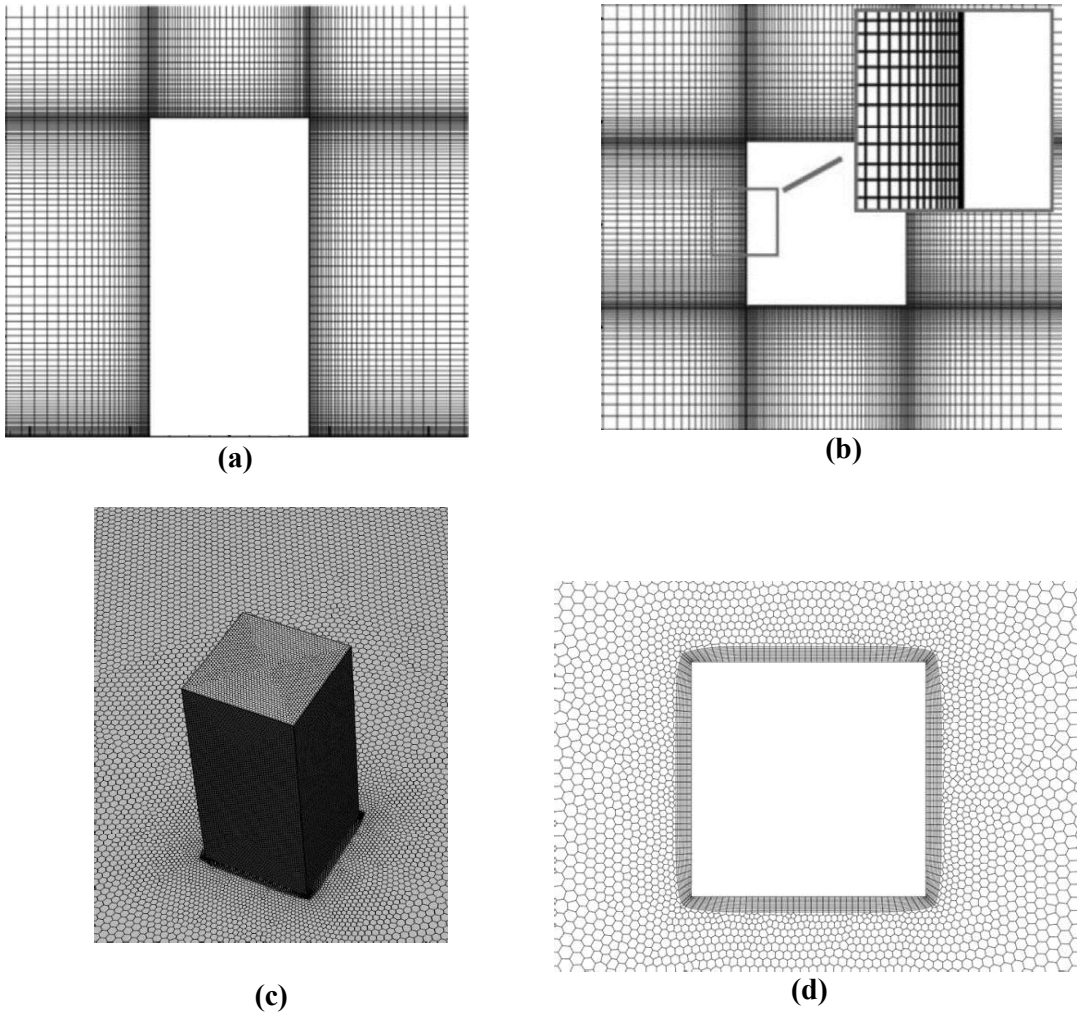

Figure 5.6 Grid distribution (a) vertical plane (b) horizontal plane (c) 3D (d) Top view

5.8 Results and discussion

5.8.1 Square plan shape model

A square plan shape with uniform cross sectional tall building is considered to validate this study using CFD simulation. The isolated model of this tall building, with dimensions L=80 mm, B=80 mm, and H=160 mm, was subjected to wind pressure directed

perpendicularly to "Face A" as depicted in Figure 5.1. As a result, Face A and Face C exhibited windward and leeward responses, generating positive and negative pressure effects, respectively, while Faces B and D, functioning as lateral sides, encountered a suction effect caused by the wind flow. The wind's initial behaviour was emulated using a velocity profile established at the inlet location, aligning with the approach taken by Liu and Niu in 2016. In this study, the pressure and force coefficients of the base model having ratio 1 : 1 : 2 (length : width : height) are compared with the CFD results of Bairagi and Dalui (2018) , AS/NZ1170: 2011, ASCE/SEI 7-10 (2010), EN: 1991-1-4 (2005), BS: 6399-2 (1997) and IS 875 (Part 3): 2015 as shown in Tables 5.2 and 5.3. The pressure contours of all the faces are shown in Figure 5.7. The velocity contours at the middle section are shown in Figure 5.8. The streamline of square shape model at 0.5H height is shown in Figure 5.9.

The pressure coefficient (C_P), The force coefficient (C_f) and Lift coefficient (C_L) are found using Equations 5.11-5.13.

$$C_p = \frac{P - P_0}{\frac{1}{2}\rho V^2} \tag{5.11}$$

$$C_f = \frac{F}{\frac{1}{2}\rho V^2 A} \tag{5.12}$$

$$C_L = \frac{F_L}{\frac{1}{2}\rho V^2 A} \tag{5.13}$$

where P is the local pressure, P_0 is the far upstream pressure, ρ is the density of air, taken as 1.185 kg/m^3, V is the mean velocity of wind , F is total wind force acting on structure, A is the plan area upon which wind force is acting, F_L is the lift force.

Table 5.2 Comparison of surface pressure coefficient(C_{pe}) on square plan building

Location	Pressure Coefficient as per					
	ANSYS CFD (Present study)	AS/NZ1170: 2011	ASCE/SEI 7-10 (2010)	EN: 1991-1-4 (2005)	BS: 6399-2 (1997)	IS 875 (Part 3): 2015
Windward side	0.78	0.8	0.8	0.8	0.76	0.8
Leeward side	-0.27	-0.5	-0.5	-0.55	-0.5	-0.25
Side walls	-0.57	-0.65	-0.7	-0.8	-0.8	0.8

Table 5.3 Comparison of force coefficient (C_f) on the vertical surface of square plan building

Force coefficient (C_f) as per					
ANSYS CFD (Present study)	Bairagi and Dalui (2018)	AS/NZ1170: 2011	ASCE/SEI 7-10 (2010)	EN: 1991-1-4 (2005)	IS 875 (Part 3): 2015
1.97	1.28	2.2	1.31	2.1	1.2

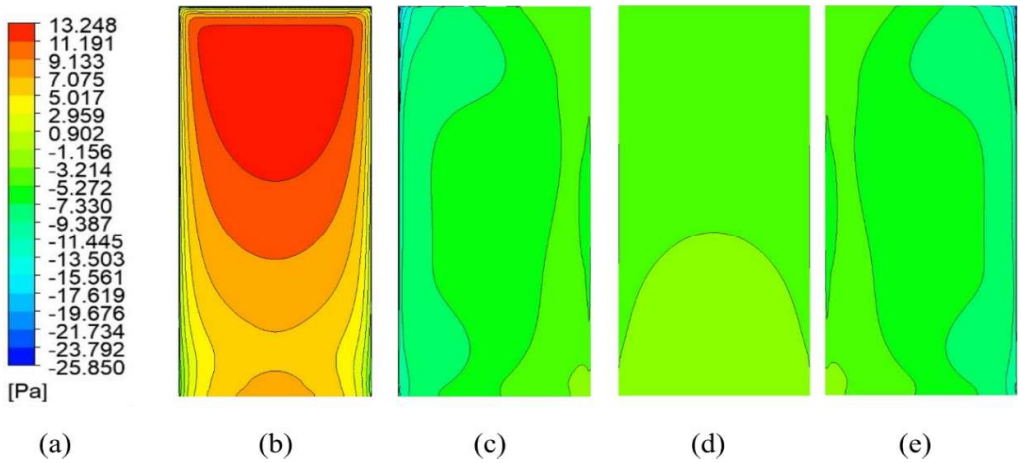

Figure 5.7 Pressure contours of square model (a) Legend (b) Face A (c) Face B (d) Face C (e) Face D

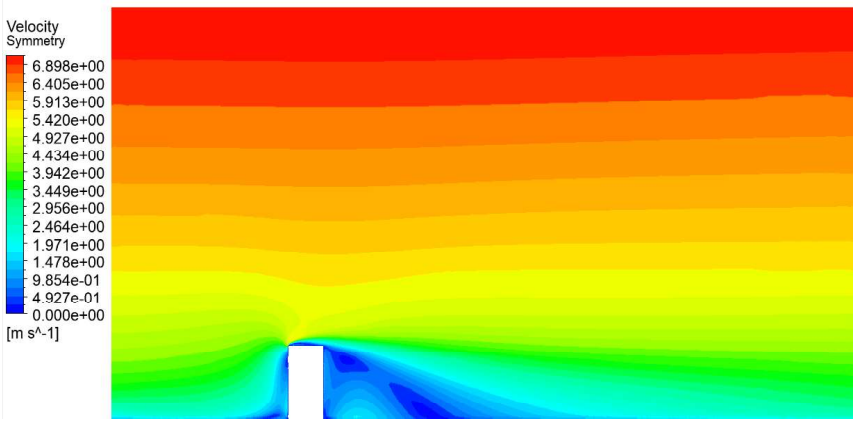

Figure 5.8 Contours of Velocity at middle section of the square model

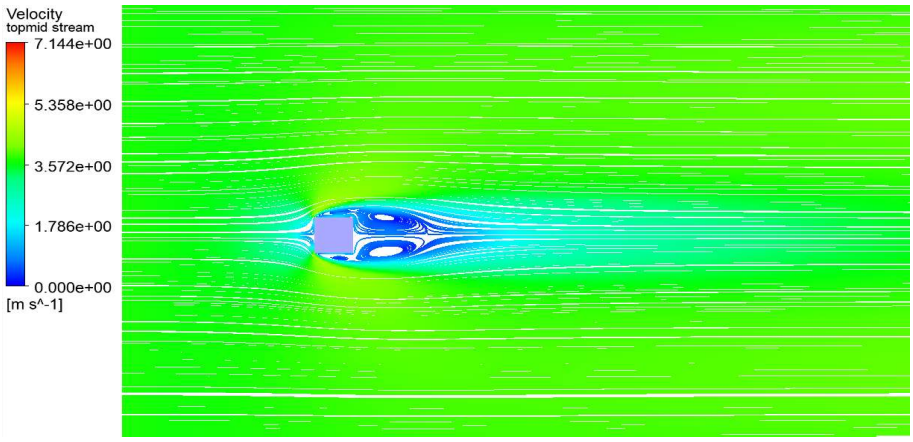

Figure 5.9 Stream line at 0.5H height of the square model

5.8.2 Pressure contour, pressure coefficients and force coefficients of different corner modification models with 5% reduction at corners

In this section, The study delves into an analysis of diverse corner modification techniques—namely chamfered, rounded, recessed, and double recessed. These changes include decreasing the length of the square model at corner by 5%. This study endeavours to effectuate a comprehensive comparative scrutiny of these corner modification methodologies. This evaluation is underpinned by the discerning utilization of pressure contour plots, as well as an assessment of pertinent coefficients, specifically pressure coefficients (C_p) and force coefficients (C_f). Table 5.4 presents the force coefficients (C_f) for various corner modification models, along with the corresponding percentage reductions resulting from the different corner modifications. It is evident from the data that chamfering stands out as the most impactful corner modification method, while recessing ranks as the least effective. However, it is worth noting that all types of corner modifications lead to a reduction in force coefficients. This collective outcome underscores the efficacy of corner modifications as a viable strategy for mitigating the exerted forces on the structure. Table 5.5 presents the lift coefficients (C_L) for various corner modification models. Lift coefficient corresponds to the across wind load of the structure. It is evident from Table 5.5 that chamfering is the best way to reduce across wind load, in the case of 5% reduction at corners.

Table 5.4 Force coefficient (C_f) of different models having 5% corner modification

Modification Type	Force coefficient (C_f)	Reduction %
Base	1.9706	-
Chamfered	1.4589	25.97
Rounded	1.5539	21.15
Recessed	1.5957	19.03
Double Recessed	1.5639	20.64

Pressure contour plots are obtained for the four faces, *i.e.*, Face A, Face B, Face C and Face D as shown in Table 5.6. Pressure coefficients (C_p) are plotted along the perimeter of the building, where, perimeter line is considered at the 2/3rd height (Bairagi and Dalui 2021) of the building. Figure 5.10 shows the pressure coefficients for various corner modification. Figure 5.10 makes it evident that face A exhibits a positive C_p, whereas all the other faces demonstrate a negative C_p.

Table 5.5 Lift coefficient(C_L) value of different models having 5% corner modification

Modification Type	Lift coefficient (C_L)	Reduction %
Base	0.082780	-
Chamfered	0.071682	13.41
Rounded	0.073865	10.77
Recessed	0.074485	10.02
Double Recessed	0.072308	12.65

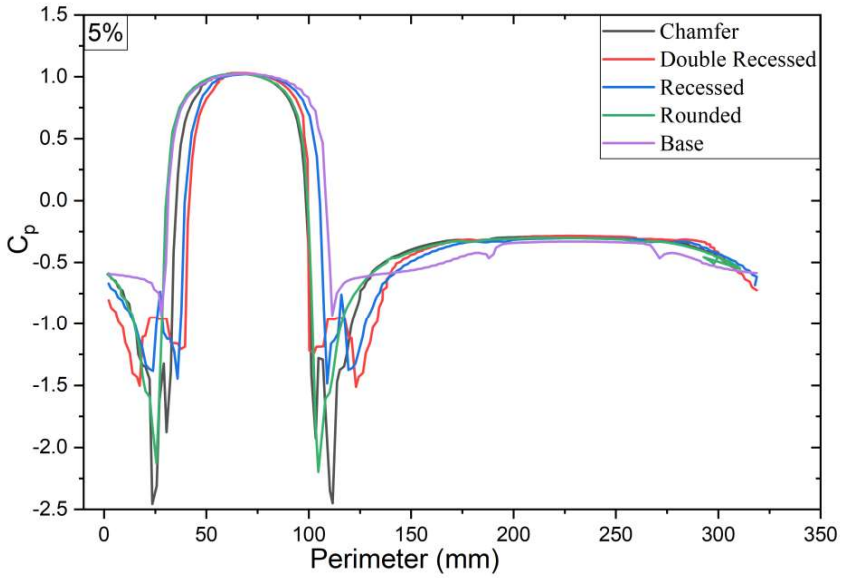

Figure 5.10 Comparison of C_p at the perimeter (2/3rd height) for 5% corner modification

Table 5.6 Pressure contours for various models of corner modifications with 5% side reduction

Modification Type	Legend	Face A	Face B	Face C	Face D
Chamfered	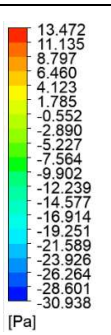	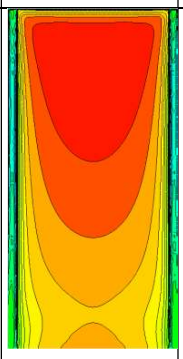	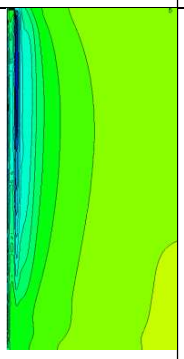	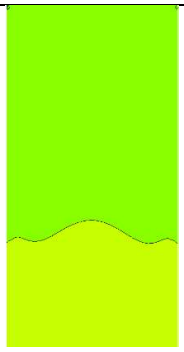	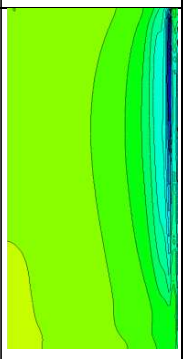
Rounded	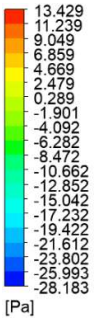	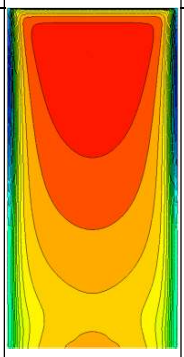	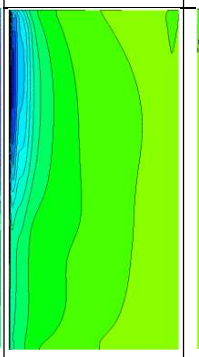	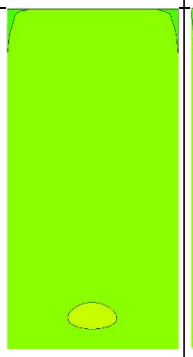	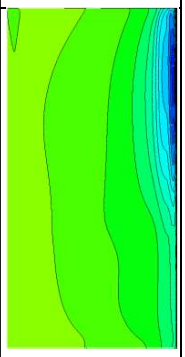
Recessed	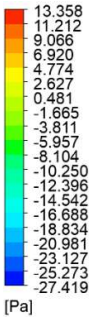	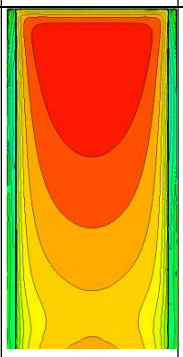	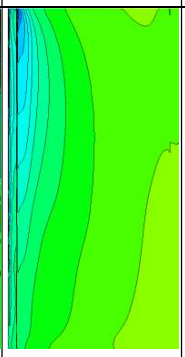	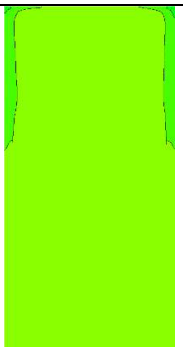	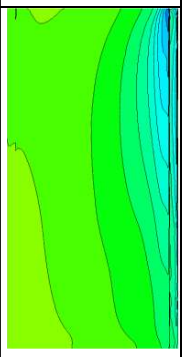
Double Recessed	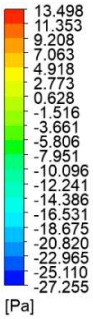	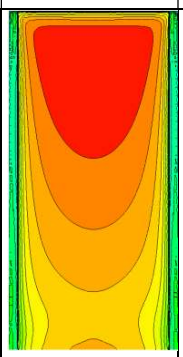	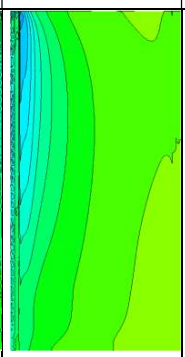	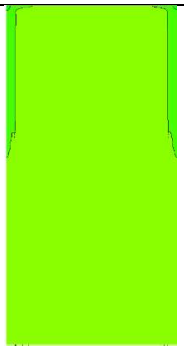	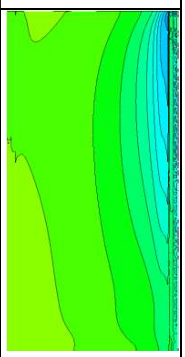

5.8.3 Pressure contour, pressure coefficients and force coefficients of different corner modification models with 10% reduction at corners

In this specific phase of the investigation, we deeply delve into an analysis of corner modification encompass a 10% reduction in the length of the square model at its corners. The principal objective of this study is to conduct a thorough and comparative analysis of different corner modification techniques. This evaluation is supported by the meticulous utilization of pressure contour plots, alongside an assessment of relevant coefficients, namely pressure coefficients (C_p) and force coefficients (C_f).Table 5.7 presents the force coefficients (C_f) for various corner modification models, along with the corresponding percentage reductions resulting from the different corner modifications. It is evident from the data that rounded corner stands out as the most impactful corner modification method, while recessing ranks as the least effective. However, it is worth noting that all types of corner modifications lead to a reduction in force coefficients. This combined results emphasizes that corner modifications are an effective strategy for reducing the forces acting on the structure. Table 5.8 presents the lift coefficients (C_L) for various corner modification models. It is evident from Table 5.8 that chamfering is the best way to reduce across wind load, in the case of 10% reduction at corners.

Table 5.7 Force coefficient (C_f) of different models having 10% corner modification

Modification Type	Force coefficient (C_f)	Reduction %
Base	1.9706	-
Chamfered	1.3260	32.71
Rounded	1.3036	33.85
Recessed	1.5739	20.13
Double Recessed	1.4925	24.26

Pressure contour plots have been generated for all four faces, namely Face A, Face B, Face C, and Face D, as detailed in Table 5.9. These plots depict pressure coefficients (C_p) along the perimeter of the models, with the perimeter line situated at two-thirds of the building's height. Figure 5.11 presents the pressure coefficient variations resulting from different corner modifications. Notably, Figure 5.11 clearly illustrates that Face A exhibits a positive C_p, while all other faces display a negative C_p.

Table 5.8 Lift coefficient(C_L) value of different models having 10% corner modification

Modification Type	Lift coefficient (C_L)	Reduction %
Base	0.082780	-
Chamfered	0.067381	18.60
Rounded	0.067600	18.34
Recessed	0.069091	16.54
Double Recessed	0.069072	16.56

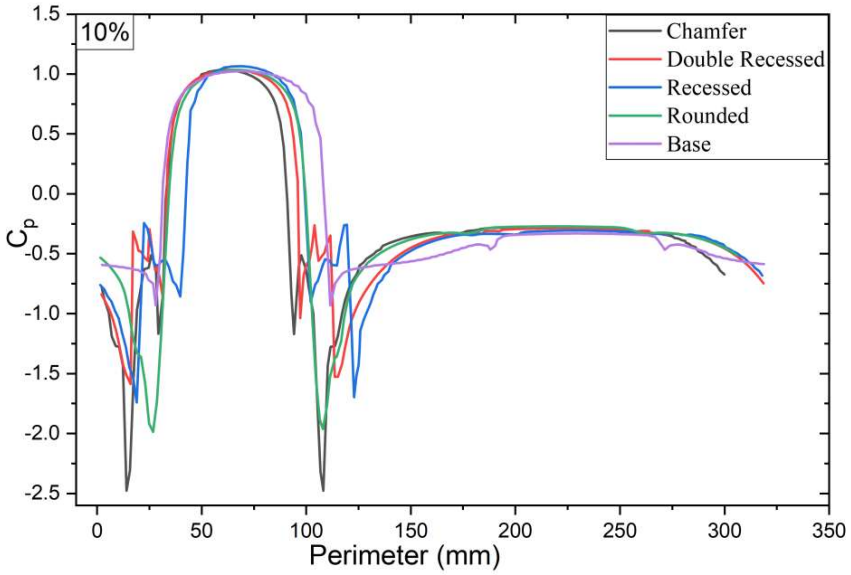

Figure 5.11 Comparison of C_p at the perimeter (2/3rd height) for 10% corner modification

Table 5.9 Pressure contours for various models of corner modifications with 10% side reduction

Modification Type	Legend	Face A	Face B	Face C	Face D
Chamfered	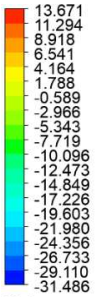	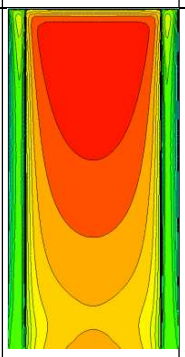	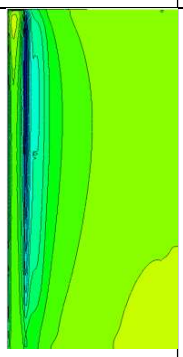	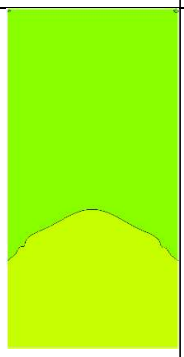	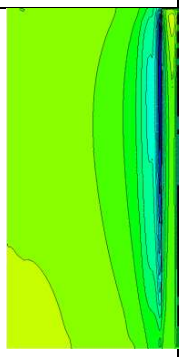
Rounded	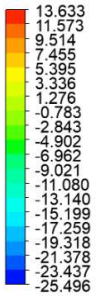	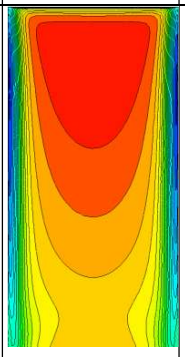	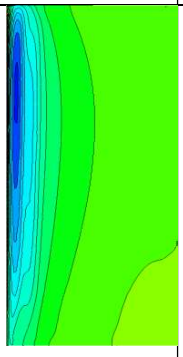	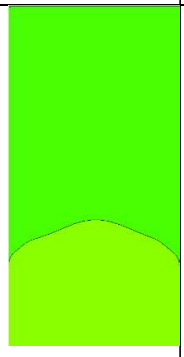	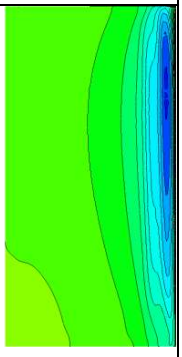
Recessed	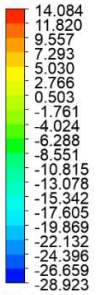	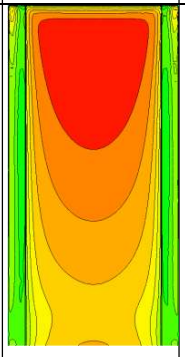	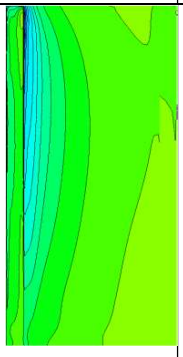	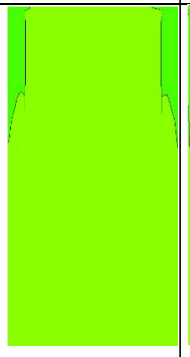	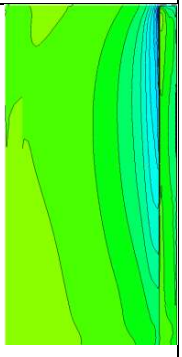
Double Recessed	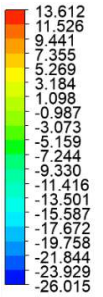	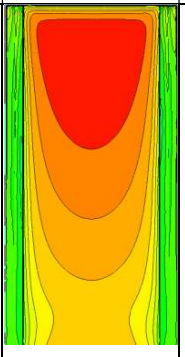	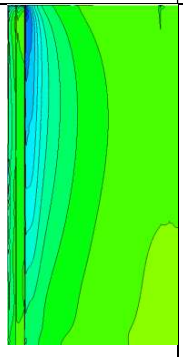	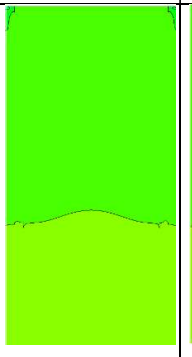	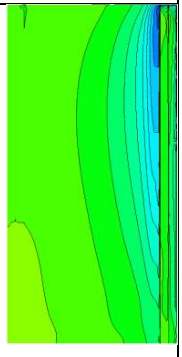

5.8.4 Pressure contour, pressure coefficients and force coefficients of different corner modification models with 15% reduction at corners

This section delves into alterations encompass a 15% reduction in the length of the square model at its corners. The core aim of this research is to conduct a comprehensive and comparative investigation of various corner modification techniques. This assessment is grounded in the precise utilization of pressure contour plots, along with an examination of key coefficients, notably pressure coefficients (C_p) and force coefficients (C_f). Table 5.10 presents the force coefficients (C_f) for various corner modification models, along with the corresponding percentage reductions resulting from the different corner modifications. It is evident from the data that rounded corner stands out as the most impactful corner modification method, while recessing ranks as the least effective. However, it is worth noting that all types of corner modifications lead to a reduction in force coefficients. This collective outcome underscores the efficacy of corner modifications as a viable strategy for mitigating the exerted forces on the structure. Table 5.11 presents the lift coefficients (C_L) for various corner modification models. Evidently, lift coefficient corresponds to the across wind load of the structure. It is evident from Table 5.11 that recessing is the best way to reduce across wind load, in the case of 15% reduction at corners.

Table 5.10 Force coefficient (C_f) of different models having 15% corner modification

Modification Type	Force coefficient (C_f)	Reduction %
Base	1.9706	-
Chamfered	1.2701	35.55
Rounded	1.2178	38.20
Recessed	1.4974	24.01
Double Recessed	1.4763	25.08

Pressure contour plots were generated for all four faces, namely Face A, Face B, Face C, and Face D, as illustrated in Table 5.12. Pressure coefficients (C_p) were graphed along the building's perimeter, with the perimeter line situated at two-thirds of the building's height. Figure 5.12 visually presents the pressure coefficient variations resulting from different corner modifications. It is readily apparent from Figure 5.12 that Face A displays a positive C_p, whereas all the other faces exhibit a negative C_p.

Table 5.11 Lift coefficient(C_L) value of different models having 15% corner modification

Modification Type	Lift coefficient (C_L)	Reduction %
Base	0.082780	-
Chamfered	0.065817	20.49
Rounded	0.065728	20.60
Recessed	0.063719	23.03
Double Recessed	0.065484	20.89

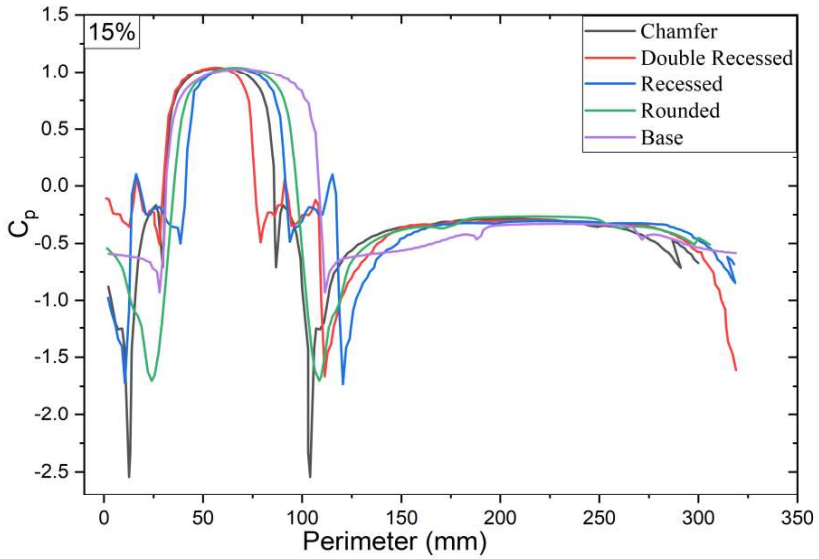

Figure 5.12 Comparison of C_p at the perimeter (2/3rd height) for 15% corner modification

Table 5.12 Pressure contours for various models of corner modifications with 15% side reduction

Modification Type	Legend	Face A	Face B	Face C	Face D
Chamfered	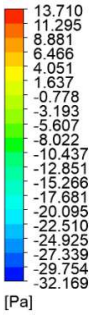	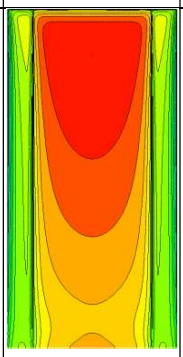	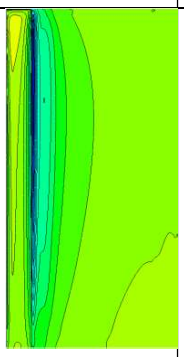	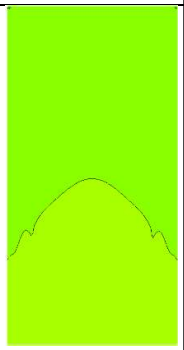	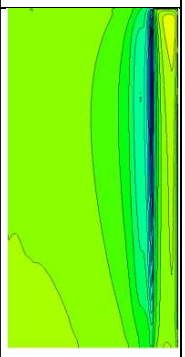
Rounded	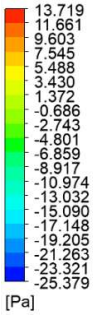	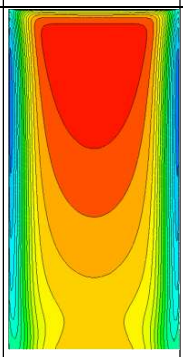	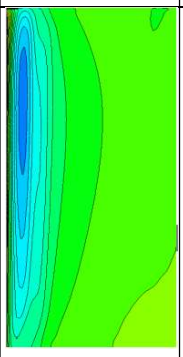	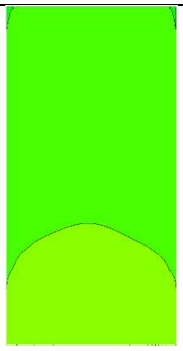	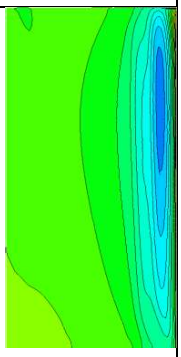
Recessed	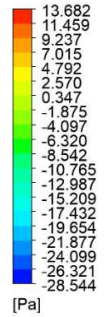	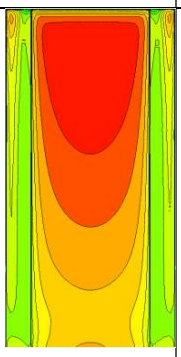	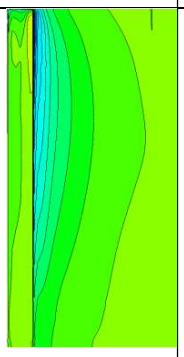	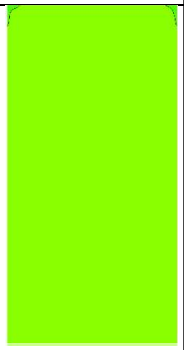	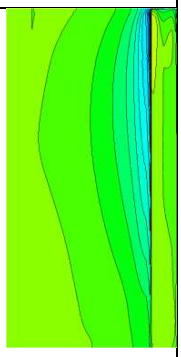
Double Recessed	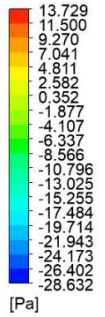	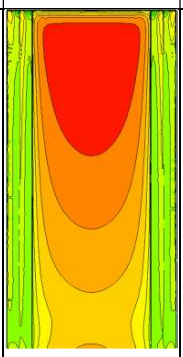	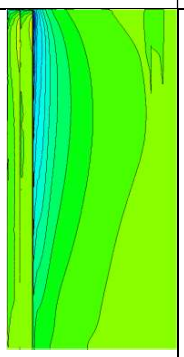	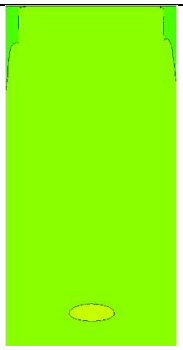	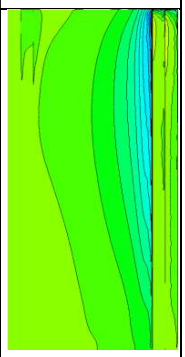

5.8.5 Pressure contour, pressure coefficients and force coefficients of different corner modification models with 20% reduction at corners

This section delves into alterations encompass a 20% reduction in the length of the square model at its corners. The main aim of this research is to conduct a comprehensive and comparative investigation into various corner modification techniques. This assessment relies on the careful utilization of pressure contour plots, as well as the evaluation of pertinent coefficients, such as pressure coefficients (C_p) and force coefficients (C_f). Table 5.13 presents the force coefficients (C_f) for various corner modification models, along with the corresponding percentage reductions resulting from the different corner modifications. It is evident from the data that rounded corner stands out as the most impactful corner modification method, while recessing ranks as the least effective. However, it is worth noting that all types of corner modifications lead to a reduction in force coefficients. This collective outcome underscores the efficacy of corner modifications as a viable strategy for mitigating the exerted forces on the structure. Table 5.14 presents the lift coefficients (C_L) for various corner modification models. It is evident from Table 5.14 that recessing is the best way to reduce across wind load, in the case of 20% reduction at corners.

Table 5.13 Force coefficient (C_f) of different models having 20% corner modification

Modification Type	Force coefficient (C_f)	Reduction %
Base	1.9706	-
Chamfered	1.2392	37.12
Rounded	1.1680	40.73
Recessed	1.5748	20.09
Double Recessed	1.5033	23.71

In this analysis, pressure contour plots were generated for all four faces—Face A, Face B, Face C, and Face D, as detailed in Table 5.15. Pressure coefficients (C_p) were graphed along the building's perimeter, specifically at the 2/3rd height of the structure. Figure 5.13 provides a visual representation of the pressure coefficient variations resulting from various corner modifications. Notably, Figure 5.13 clearly illustrates that Face A exhibits a positive C_p, while all other faces display a negative C_p.

Table 5.14 Lift coefficient(C_L) value of different models having 20% corner modification

Modification Type	Lift coefficient (C_L)	Reduction %
Base	0.082780	-
Chamfered	0.062159	24.91
Rounded	0.064364	22.25
Recessed	0.060499	26.92
Double Recessed	0.062158	24.92

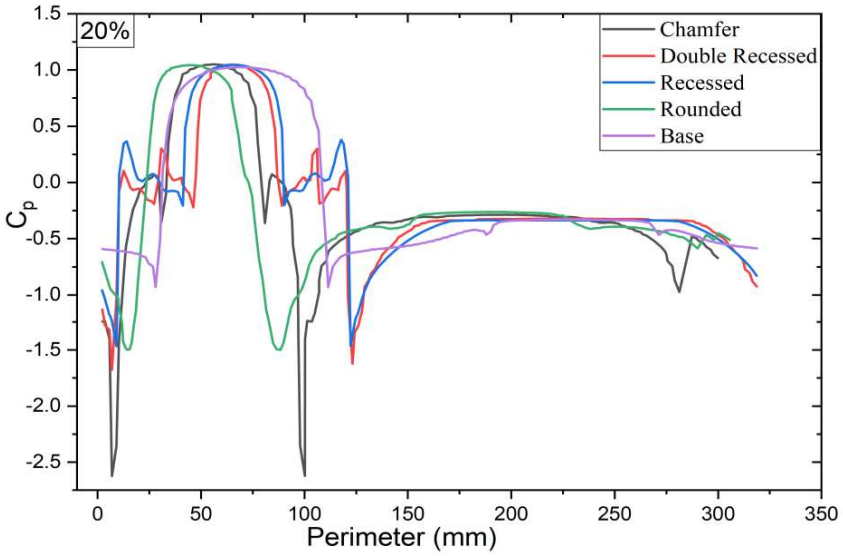

Figure 5.13 Comparison of C_p at the perimeter (2/3rd height) for 20% corner modification

Table 5.15 Pressure contours for various models of corner modifications with 20% side reduction

Modification Type	Legend	Face A	Face B	Face C	Face D
Chamfered	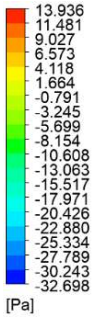	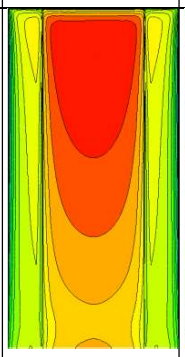	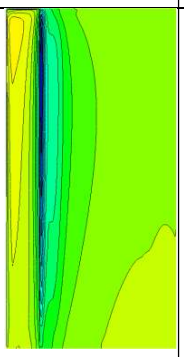	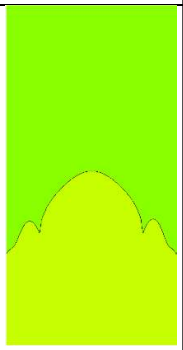	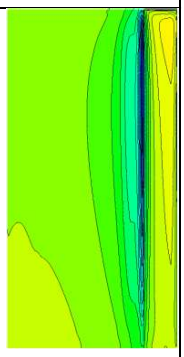
Rounded	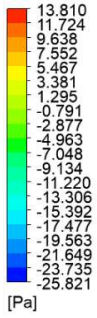	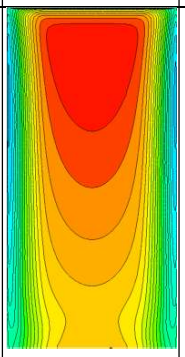	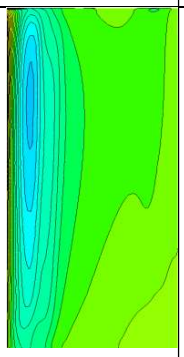	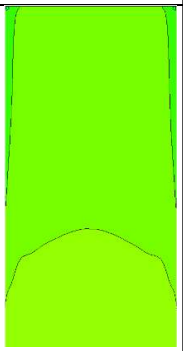	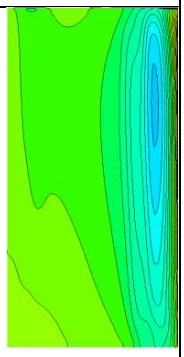
Recessed	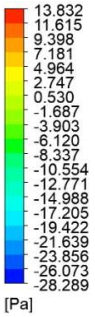	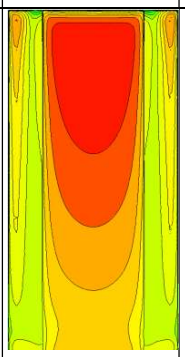	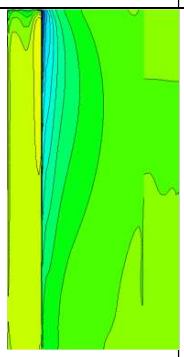	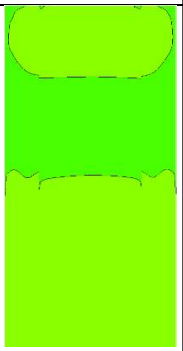	
Double Recessed	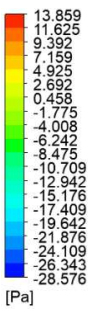	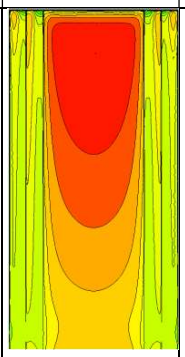	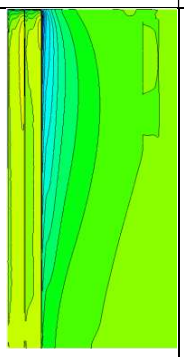	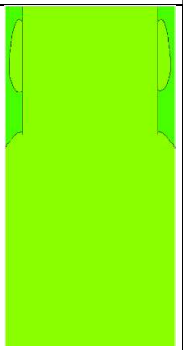	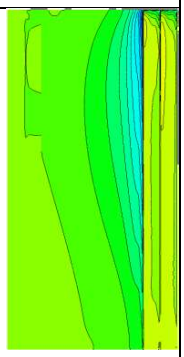

5.9 Concluding remark

In conclusion, this study has rigorously examined the influence of corner modifications on both along and across wind load. By employing four distinct corner modification strategies—chamfered, rounded, recessed, and double-recessed—the study revealed invaluable insights into the aerodynamic characteristics of tall square-plan buildings. Through CFD analysis and subsequent comparisons with the original square model, a comprehensive picture has emerged. Notably, These findings collectively illuminate the potential of corner modifications as efficient strategies for mitigating wind loads on square-plan tall buildings. Key observations of the study are discussed below:

- At a 5% corner reduction, chamfering emerges as the optimal approach, resulting in a substantial 25.97% reduction in overall wind load and a noteworthy 13.41% reduction in across-wind load.
- In cases with a 10% reduction, rounded and recessed corners excel, attaining reductions of 33.85% and 32.71% in overall wind load, respectively. Meanwhile, chamfered and rounded corners demonstrate commendable performance in decreasing across-wind load, with reductions of 18.60% and 18.34%, respectively.
- Furthermore, for a 15% reduction in corners, rounded and chamfered corners prove most effective in minimizing overall wind load with reductions of 38.20% and 35.50% respectively. Recessed corners, on the other hand, excel in reducing across-wind load, achieving a substantial 23.03% reduction.
- Lastly, when corners are reduced by 20%, rounded corners display exceptional efficacy in diminishing overall wind load by 40.73%, while recessed corners effectively curtail the across-wind load by 26.92%.